ON THE EXPERIMENTAL SIMULATION OF EGS RESERVOIRS USING A HEATED TRUE-TRIAXIAL APPARATUS

Luke Frash[1], Marte Gutierrez[1], Jesse Hampton[1]

[1]Colorado School of Mines, 1610 Illinois St, Golden, CO, 80401, USA

lfrash@mines.edu

Keywords: *Enhanced Geothermal Systems (EGS), True-Triaxial, Hydraulic Fracture, Acoustic Emissions (AE), Laboratory.*

ABSTRACT

Geothermal energy technology has successfully provided a means of generating stable base load electricity for many years. However, implementation has been spatially limited to rare high quality traditional resources possessing the combination of a shallow high heat flow anomaly and an aquifer with sufficient permeability and fluid recharge. Enhanced Geothermal Systems (EGS) technology has been proposed as a potential solution to enable additional energy production from the much more common non-traditional resources. To advance this technology development, a heated true-triaxial load cell with a high pressure fluid injection system has been developed to simulate an EGS system from stimulation to production. This apparatus is capable of loading a 30x30x30 cm rock sample with independent principal stresses up to 13 MPa while simultaneously providing heating up to 180 ºC. Multiple orientated boreholes of 5 to 10 mm diameter may be drilled into the sample while at reservoir conditions. This allows for simulation of borehole damage as well as injector-producer schemes. Dual 70 MPa syringe pumps set to flow rates between 10 nL/min and 60 mL/min injecting into a partially cased borehole allow for fully contained fracturing treatments. A six sensor acoustic emission (AE) array is used for geometric fracture location estimation during intercept borehole drilling operations. Hydraulic sensors and a thermocouple array allow for additional monitoring and data collection as relevant to computer model validation as well as field test comparisons. The results from preliminary tests inside and outside of the cell demonstrate the functionality of the equipment while also providing some novel data on the propagation and flow characteristics of hydraulic fractures themselves. Fully characterized test sample materials used include generic cement grout, custom high performance concrete, granite, and acrylic. Fracturing fluids used include water, brine, and Valvoline® DuraBlend® SAE 80W90 oil.

1. INTRODUCTION

The potential of EGS is well documented in the MIT led study titled “The Future of Geothermal Energy” (Tester et al., 2006). With this technology, unconventional deep hot dry rock (HDR) reservoirs are engineered with drilling and stimulation techniques to create a heat mining system for base load energy production. The methods needed for enabling EGS energy production also have the ability to improve production from traditional geothermal resources which are already being harvested today.

To provide the EGS reservoir stimulation, one of the most promising techniques is hydraulic fracturing. This method utilizes high pressure fluid injection into targeted reservoir intervals to enhance permeability and generate new flow paths through enhancing existing fractures and creating new fractures. With the installation of an injector-producer well scheme, the physical limitations of natural reservoir recharge and stored harvestable fluids may be overcome and a productive reservoir may be the end result. Hydraulic fracturing has been proven effective as a stimulation technique by the oil and gas industry since its first implementation in 1947 (Clark, 1949).

Currently, only a small number of EGS field trials have been performed due to the high economic risk of the procedure and the significant probability of failure. Thus, performing controlled EGS experiments in the laboratory setting may be able to provide some of the crucial data and experience needed for advanced fracture model calibration and full scale testing in the field. This is especially true considering that most hydraulic fracturing design techniques, as developed by the petroleum industry, are more dependent upon historical data than on theoretical analysis (Green et al, 2008). In the case of EGS development, this historical data does not yet exist in sufficient quantities.

To fill the knowledge gap, laboratory scale EGS reservoir testing is being performed at the Colorado School of Mines using a heated true-triaxial apparatus. Some completed test results and observations are presented along with technical information on the equipment and procedures used. Focus is given to series of tests performed on a hydraulically fractured granite sample with a binary injector-producer borehole scheme installed.

2. EQUIPMENT DETAILS AND SPECIFICATIONS

The laboratory scale EGS simulation equipment consists of four main subsystems being a heated true-triaxial cell, a high pressure hydraulic injection system, a multi-component data acquisition system, and sample materials and characterization equipment.

2.1 Heated True-Triaxial Cell

The true-triaxial cell, as shown in Figure 1, is capable of loading large 30x30x30 cm blocks with independently controlled principal stresses of up to 12.5 MPa using three independently pressurized Freyssinet 350 mm flat jacks. Externally mounted flexible silicone rubber heaters with PID control allow for dual-zone heating with separate set points for the lateral and vertical heating elements. In other terms, this equipment allows for the simulation of an EGS reservoir at approximately 460 m depth and up to 180 ºC temperature.

An orientated rotary-hammer drill press, shown in Figure 2, is used to cut boreholes into the sample at user selected positions and angles while the sample is held at pressure and temperature. This procedure allows for strategic borehole installations that are specific to the test and the particular stimulated fracturing plane as observed with

acoustic emission (AE) visualization methods. Borehole damage is replicated by using percussive drilling into the loaded sample instead of the more common cast-in-place pre-drilled borehole methods (Behrmann and Elbel, 1991, de Pater et al., 1994, Ishida et al., 2004, Wieland et al., 2006). The borehole was typically drilled with one upper cased segment having a maximum outside diameter of 10 mm and a second uncased fracturing interval having a typical diameter of 5.6 mm, as shown in Figure 4. These dimensions were selected to be as small as possible to allow for the most effective EGS reservoir simulation within the confines of the 30x30x30 cm cubical sample blocks.

Figure 1: Heated true-triaxial cell with sample installed.

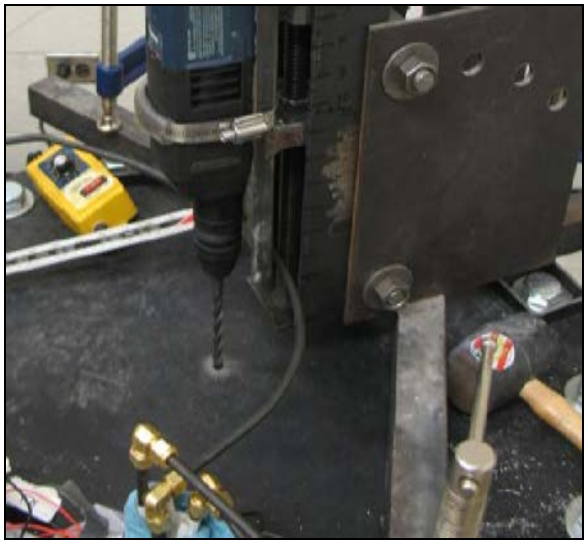

Figure 2: Orientated percussive drilling of an injection borehole using a custom drill press.

2.2 High Pressure Hydraulic Injection System

A programmable hydraulic injection system is used for both hydraulic fracture stimulation and post-fracture flow analysis. Precision high pressure flow is provided by a dual 65DM Teledyne Isco syringe pump system, a series of pneumatic-hydraulic automated valves, and a custom pump control program developed with LabVIEW. This system is capable of providing pressures up to 70 MPa and precise controlled flow rates between 10 nL/min and 60 mL/min with a flow stability of ±0.3% from the set point. A diagram of the hydraulic system is provided in Figure 3.

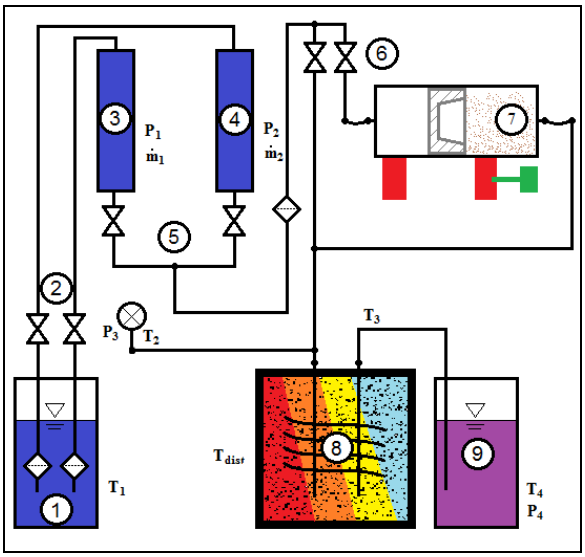

Figure 3: Diagram for the hydraulic fracturing system showing the inflow fluid reservoir (1), pneumatic actuated continuous flow valve system (2 and 5), dual high pressure syringe pumps (3 and 4), clean to slurry valve switching system (6), rotationally mixed hydraulic to hydraulic piston actuator (7), sample block (8), outflow reservoir (9), and general arrangement of select sensor systems.

Some of the programmable capabilities of the system include:

- Stepwise continuous constant flow or pressure.
- Controlled switching between clean and slurry fluid injection.
- Conditionally dependent operation with real time external data referencing capability.

To seal the injection tubing into the borehole, threaded 316 SS tubing was grouted into a 10 mm outside diameter borehole using Loctite® Rapid Mix 5-Minute epoxy. The epoxy grout was delivered downhole using water-softened 00-size gelatin capsules to avoid the potential of bonding the casing to the true-triaxial cell's top lid. After reaching a 24 hr cure, an uncased 5.6 mm diameter interval was drilled through the bottom of the casing and into the sample. Figure 4 shows a diagram of this sealing method.

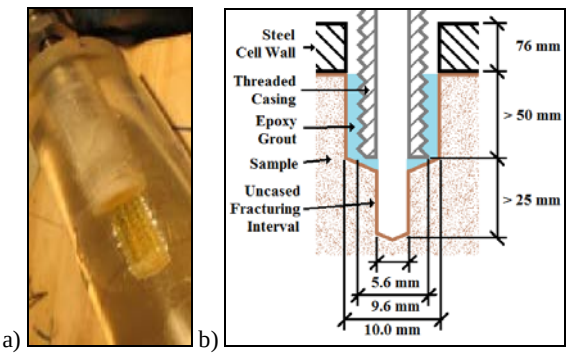

Figure 4: Borehole sealing method applied in acrylic (a) with typical dimensions shown (b).

2.3 Multi-Component Data Acquisition System

To monitor and control the equipment and system processes a multi-channel multi-function National Instruments CompactDAQ was used with 16 strain gage channels, 16 CJC thermocouple channels, 8 voltage channels, 8 current channels, and 4 multi-function channels. The attached sensors included 2 Omega® PX309-10KG5V pressure transducers for monitoring the injection wellhead pressure and intermediate principal sample confining stress, 1 Omega® PX309-3KG5V pressure transducer for monitoring the minimum principal stress, 1 Omega® PX40-50mmHG pressure transducer for monitoring the production reservoir fill level and flow rate, 1 Omega® LD621-30 linear displacement transducer for auxiliary use, and 1 Humboldt HM2310.04 linear strain transducer also for auxiliary use. Omega® Type-T thermocouples, fabricated in-house, were positioned at the hydraulic temperature monitoring positions as indicated in Figure 3, inside the bottom of the injection and production boreholes, and in a high-coverage grid arrangement on the surface faces of the sample inside the cell. When used, strain gages were embedded onto the faces of the sample to monitor stress uniformity. Additional data was collected from the Teledyne Isco pump controller for information about hydraulic system operation including flow rates, pressures, valve positions, and general pump status.

To monitor the fracturing process and provide real-time location estimation for the generated hydraulic fractures, a 6-sensor piezoelectric acoustic emission (AE) monitoring system, obtained from Physical Acoustics Corporation, was installed inside the cell with sensors contacting the faces of the sample in an arrangement to achieve maximum volumetric coverage. Figure 5 shows an AE sensor installed into a 25 mm thick loading platen where it was protected from the high loading stresses being applied to the sample. Thin packing foam wafers were inserted between the sensor body and the steel housing to dampen external acoustic noise effects and provide a soft spring reaction for any movement that would occur during loading and unloading processes. In general, this platen serves as a movable interface between the pressurized flat jack and the sample inside the cell.

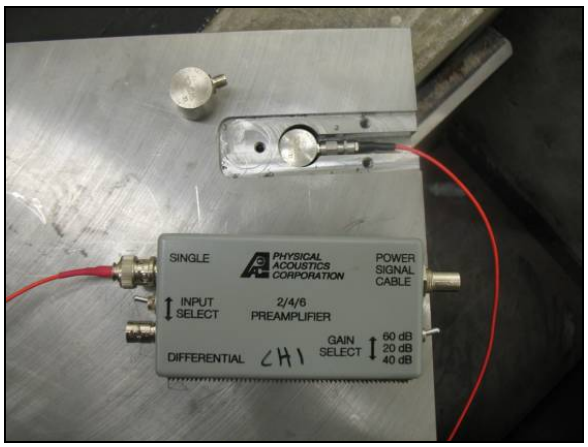

Figure 5: AE sensor installed in a loading platen.

2.4: Sample Materials and Equipment

Four material types have been used for this project including medium strength concrete grout, ultra-high strength low permeability concrete, locally obtained Colorado Rose Red Granite, and acrylic glass. Each of these materials was tested for a variety of mechanical, thermal, and acoustic properties to provide a reference for future field data comparison. A general summary of the measured properties for selected materials has been provided in Table 1. The uniaxial compression strength (UCS), elastic modulus (E), Poisson's Ratio (ν), and indirect tensile strength (BTS) testing was performed using a specially instrumented ELE Accu-Tek™ 250 concrete load frame. Thermal conductivity (k_T) measurements were performed using a divided bar apparatus available through the Colorado Geological Survey (Macartney and Morgan, 2011). Volumetric specific heat capacity (C_V) was obtained using an insulated calorimeter. Acoustic compression (V_P) and shear (V_S) wave velocities were obtained using a piezoelectric pulse transmitter-receiver apparatus with oscilloscope monitoring. Porosity (Φ) and matrix density (ρ_{dry}) were measured using a 70% vacuum desiccator, 110ºC oven, and digital mass balance.

Table 1: Material properties.

	Medium Strength Concrete	Ultra-High Strength Concrete	Colorado Rose Red Granite
UCS (MPa)	50-60	123-154	152 ± 19*
BTS (MPa)	2.2-2.7	4.0-6.0	7.5 ± 1.8*
E (GPa)	9.5-10.5	20-30	57*
ν	-	-	0.32*
ρ_{dry} (kg/m^3)	1950	1970	2650
k_T (W/m-K)	-	1.60 ± 0.02	3.15 ± 0.05
C_V (kJ/m^3-K)	2013 ± 145	1820 ± 146	2063 ± 92
Φ	0.30-0.31	0.15-0.23	0.006-0.008
V_S (mm/μs)	2.48	2.54	2.62
V_P (mm/μs)	3.41	3.89	4.45

* (EMI, 2010)

For post-test analysis, diamond cores and cut cross-sections were used. The cores were taken to remove the borehole casing and observe the near wellbore fracture geometry. Next, cross-sections were cut using a 0.9 m diameter diamond table saw. An example cross section taken from an unconfined granite sample hydraulic fracturing test is shown in Figure 6. Cross sections such as these allowed for physical measurements of the fracture locations, fluid permeation depths, and verification of AE fracture location estimations. Fluid pathways and permeation depths were most visible on tests using oil as the fracturing fluid due to staining of the sample material. Compiling fracture geometry data from consecutive cross sections allows for three-dimensional imaging of entire stimulated fracture networks. As evident in Figure 6, these networks are expected to be very complex due to the heterogeneities in natural rock and concrete samples.

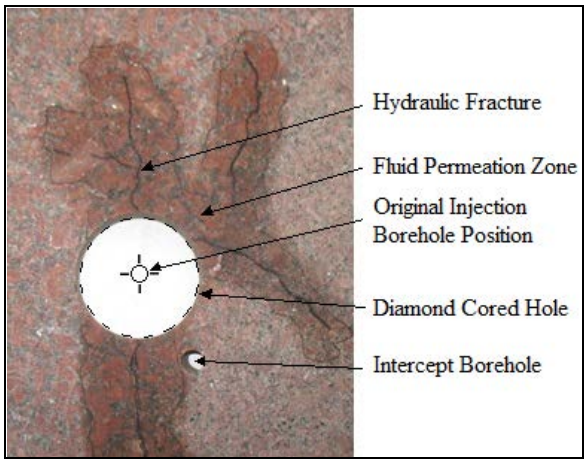

Figure 6: Cross-section from an unconfined granite hydraulic fracturing test.

3. TEST RESULTS AND OBSERVATIONS

Using this equipment, an ongoing series of hydraulic fracturing stimulation and reservoir characterization testing is being performed to obtain new data for EGS technology advancement. While hydraulic fracturing experiments have been performed in more than 11 different boreholes and four different materials, focus will be given to a granite hydraulic fracturing test where an orientated intercept borehole was drilled to create a producing heated EGS reservoir. The results of the EGS simulation experiment can be divided into several key phases including sample preparation, primary hydraulic fracturing, drilling the fracture intercept borehole, and fracture reopening and flow.

3.1 Sample Preparation

For this test, a block of Colorado Rose Red Granite, as documented in Figure 7, was loaded into the true-triaxial cell and slowly heated to an average internal temperature of 50 ºC over the span of four days. After the target temperature was reached, the sample was pressurized with confining stresses of 12.5, 8.3, and 4.1 MPa for the vertical, maximum horizontal, and minimum horizontal stresses respectively. The AE monitoring system was active throughout the loading process to identify if any mechanical shearing or thermal fracturing events had occurred. In this case, the AE data produced a large scatter of events with no significant clustering which indicated that uniform loading had successfully been achieved and no significant fracturing events had occurred.

While loaded, a centered vertical borehole was drilled into the sample, a 107 mm deep casing interval was installed, and a 73 mm uncased interval was drilled for a final injection well depth of 180 mm. It is important to note that drilling the borehole while the sample is under load is a unique system capability that allows for laboratory simulation of a borehole damage zone. This process creates small fractures near the borehole, as has been clearly observed in acrylic testing (Gutierrez et al., 2012), which may serve as fracture initiation locations. Simultaneously, the drilling process also fills these micro fractures with fines which are believed to have some effect on fracture self propping as well as near wellbore tortuosity and skin factor. Additional investigation may be necessary to better understand how the borehole damage zone influences hydraulic fracture initiation, growth, and closure.

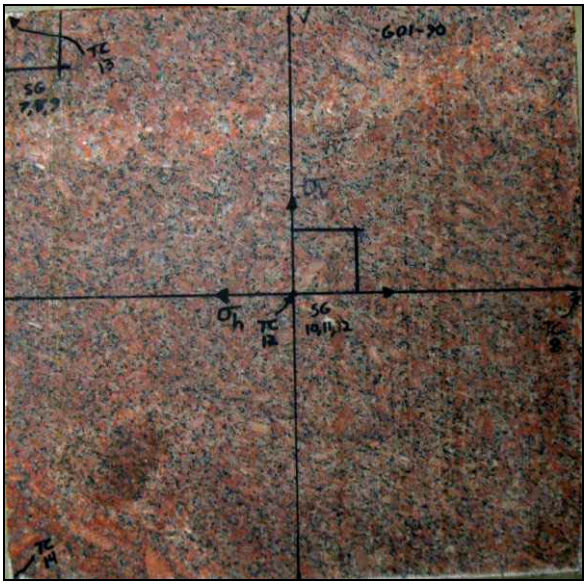

Figure 7: Pre-test image of the granite sample used for EGS reservoir simulation experiments.

3.2 Primary Hydraulic Fracturing

Primary hydraulic fracture breakdown was achieved using oil injection at a constant flow rate of 0.05 mL/min. Valvoline® Durablend® SAE 80W90 gear oil was used as the fracturing fluid due to its high viscosity value and publicly available fluid properties. At the injection temperature of 50 ºC, this fluid has an approximate dynamic viscosity of 71.5 cP as estimated using the published product information in conjunction with the Walther Equation specified in ASTM D341 (2009). The importance of using high viscosity fluid for laboratory hydraulic fracture experiments is well documented (de Pater et al., 1994, and Ishida et al., 2004). In this case, using a high viscosity fluid provided the important benefits of better fracture growth control for improved probability of containment and a more predictable fracture orientation as the propagation would be less influenced by natural heterogeneities in the granite sample.

A plot of the hydraulic data for primary breakdown is shown in Figure 8. During this test, the pump was stopped shortly after breakdown in an attempt to keep the fracture fully contained while real-time AE events were observed to be approaching the edges of the sample. Continued AE activity was observed even after pumping was stopped which indicated continued fracture propagation. Therefore, to forcibly halt the fracture growth, the flow rate was briefly reversed to pull fluid out of the fracture and then held in the stopped position. At this time, a significant pressure rebound was observed which may offer some insight into fracture dynamic fluid storage behavior with additional investigation. Ultimately, the observation of a negligible flow rate during post-fracture constant pressure testing at 2000 kPa verified that a fully contained fracture had been generated.

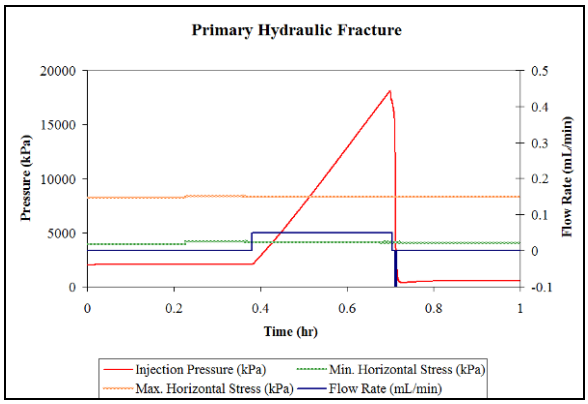

Figure 8: Hydraulic data plot for primary fracture.

Analysis of the AE source location data collected during this primary hydraulic fracture test revealed that a contained and planar fracture propagated from the borehole in a direction perpendicular to the minimum horizontal confining stress. Additionally, the fracture appeared to have a single dominant wing as evident by the AE cloud being most prominent on only one side of the borehole. Figure 9 shows orthogonal plots of the three-dimensional AE event source location results for the test. This analysis used six-sensor location regression and filtered the results to only contain events with a correlation coefficient greater than 0.75 and amplitude greater than 25 dB. On this plot, the circle diameters are directly proportional to the amplitude of the corresponding event. Also, the color shading corresponds to the correlation coefficient of each event with dark red circles having higher correlation. The two-segment centered vertical injection borehole is clearly visible on the front and side view plots.

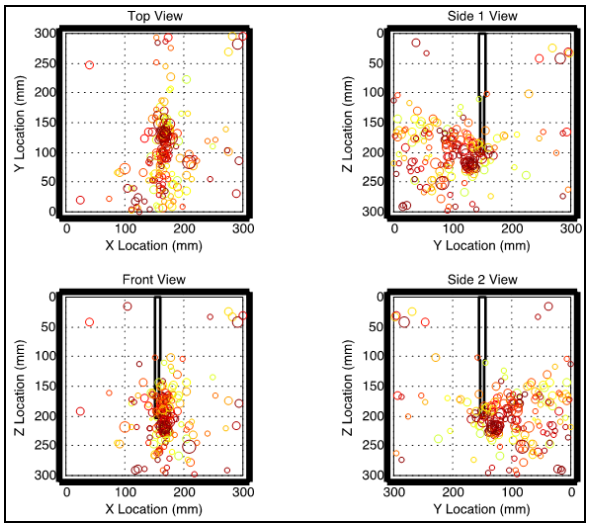

Figure 9: AE event source locations during primary hydraulic fracture.

Extending the AE analysis by application of moment tensor methods (Ohtsu, 1995), information was obtained about the fracturing mode for some of the recorded AE events. As shown in Table 2, only about 11% of the total number of recorded events could successfully be classified with a reasonable level of certainty. At a glance, the tensile failure mode appears to be dominant during this fracturing stage but uncertainty associated with the low percentage of classifiable events effectively reduces the confidence of any conclusions which could possibly be derived from these figures.

Table 2: AE Event Classification Statistics

AE Event Category	Number	% Total	% Classi.
Total Events Located	726	100	-
Classifiable Events	81	11.2	100
Tensile Events	39	5.4	48.1
Shear Events	28	3.9	34.6
Mixed Mode Events	14	1.9	17.3

3.3 Drilling the Fracture Intercept Borehole

Using AE source location data, an estimate of the fracture geometry was obtained and an optimal intercept borehole position was selected as shown in Figure 10. Here, the intercept borehole trajectory, drilled at 30º from the vertical axis, can be seen penetrating through the expected fracture surface. A high-angle drilling orientation was used to maximize the probability of achieving a successful intercept after considering AE source location uncertainty and drilling system tolerances. Also, the uncased 10 mm diameter intercept borehole was drilled deeper than the expected intercept location to further increase the probability of successful hydraulic connection. In the figure, the best estimate of the fracture plane was plotted using a smoothed cubic interpolation surface function fitted to events with both high-amplitude and high-correlation. After drilling was completed, the borehole was swabbed and positive indication of fracturing oil was recovered, thus indicating that the intercept was successful.

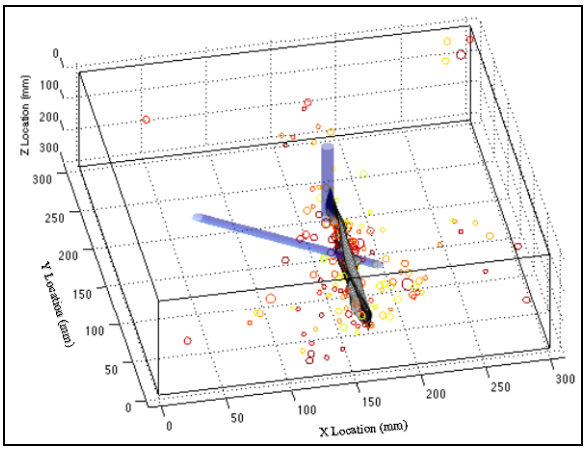

Figure 10: AE generated fracture surface of initial hydraulic fracture.

3.4 Fracture Reopening and Flow

With the completion of the simulated EGS reservoir, flow experiments were performed to characterize the hydraulic properties of the reservoir. These experiments included constant pressure steady state injection, constant flow rate injection for fracture reopening, stepped constant pressure injection, and constant flow rate water injection. The results obtained from these tests ultimately verified that a hydraulic circuit was present inside of the sample connecting the injection borehole to the production borehole through the stimulated hydraulic fracture.

Initially, constant low-pressure steady-state injection was performed using specified pressures of 2000, 3000, or 4000 kPa. The pressures were intentionally kept below the minimum principal stress to avoid the potential for continued propagation or fracture reopening. The results from these tests demonstrated that the achievable stable flow rates with the primary hydraulic fracture geometry were negligible and thus the reservoir remained non-producing. While this information confirmed that the stimulated fracture geometry was fully contained as desired, it also indicated that the connection between the injection and production borehole was too tight to pass any significant amount of fluid through. It is expected that a significantly higher post-fracture hydraulic conductivity would occur if proppant had been used during the primary fracturing stage.

To enhance the hydraulic connection of the binary borehole system, two fracture reopening stages were performed with stepped constant pressure injection tests executed in between for diagnostic purposes. Figures 11 and 12 show plots of the hydraulic data obtained from the first and second fracture reopening stages respectively. Both of these plots clearly show classic hydraulic fracture reopening behavior (Weijers, 1994) with a nearly linear pressure rise followed by a rapid breakdown event and pseudo-steady fracture propagation at an elevated pressure. Comparing the similar magnitude peak pressures of 18.1, 15.4, and 17.4 kPa, observed for the primary fracture, first reopening, and second reopening events respectively, suggests that fracture toughness was not a dominant factor in fracture propagation so scaling criterion suggested in the literature (Johnson and Cleary, 1991, and de Pater et al., 1994) are likely to be satisfied even with intact granite as the testing material.

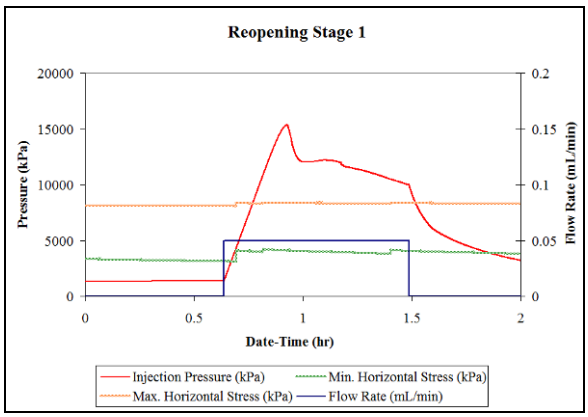

Figure 11: First fracture reopening event.

An orientated view of the AE source location data as observed for the first reopening stage is shown in Figure 13. Comparing this figure to the results shown in Figure 10 and the data from the second reopening stage, it is apparent that most of the fracture growth occurred during the first reopening stage along the bottom and two horizontal extremities of the initial fracture plane. Additionally, the close proximity of the AE events to the boundaries of the sample suggests that the stimulated fracture may no longer be fully contained and lower fluid recovery efficiency may result. This situation, while not ideal, more closely resembles the high fluid loss systems as encountered at field test sites such as Hijiori, Japan (Swenson et al., 1999). For the final fracture geometry, the smaller wing of the initial fracture appeared to have extended to approximately match the dominant wing length, thus creating a planar bi-wing fracture.

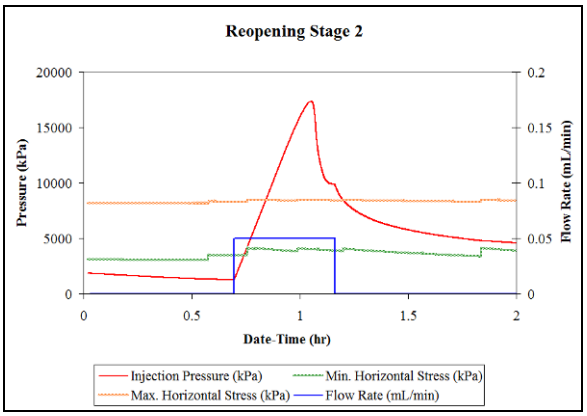

Figure 12: Second fracture reopening event.

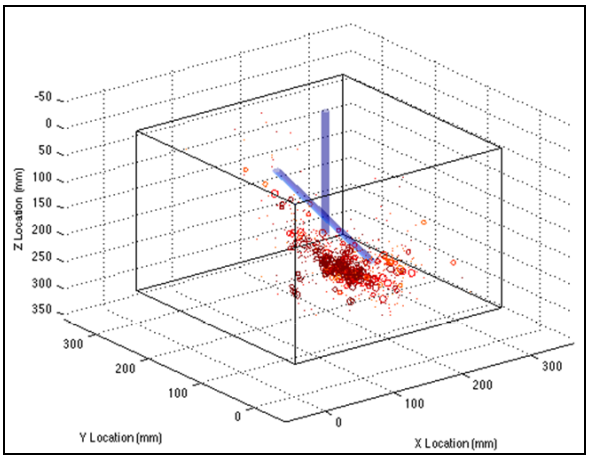

Figure 13: Three dimensional view of AE event source locations during first fracture reopening stage.

Comparing the AE count frequency data with the pressure data, as shown in Figure 14, significant increases in AE activity were found to occur just after portions of the hydraulic data where the second derivative of injection pressure with time was negative. Thus, from observing the real-time rate of slope change in the pressure data, it may be possible to anticipate a major fracture growth event before it occurs. Also, using a technique such as this allows for an improved understanding of fracture growth behavior in heterogeneous systems during the time between fracture initiation and shut-in. During this time, the second-order analysis could be used to identify distinct breakdown events occurring after the initial breakdown as could be expected with multi-wing fracture systems or the opening of intersected fissures, joints, or fault zones. In this laboratory case, the analysis was performed using an 11-second backward linear regression approach to obtain an estimate of the first pressure derivative, as could be used in real-time applications.

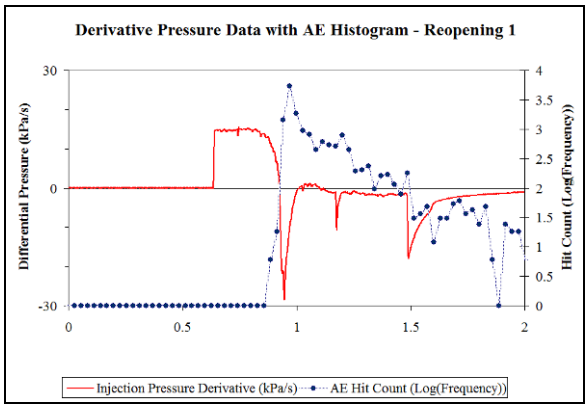

Figure 14: First time derivative of pressure with AE hit count histogram for the first fracture reopening stage.

To evaluate the effectiveness of each fracture reopening stage, stepped constant pressure injection tests were performed. In these tests, fluid was injected into the sample with PID controlled pressure at 1000 kPa increments with 30 minute duration. An example of the pressure data from a step pressure test performed after the second reopening event is provided in Figure 15. For each constant pressure increment, the resulting steady state pressure and flow rate measurements are averaged to estimate the pressure dependent flow characteristics of the stimulated reservoir. These values were useful reference points during later controlled constant flow tests where fracture reopening and extension pressures were not desired.

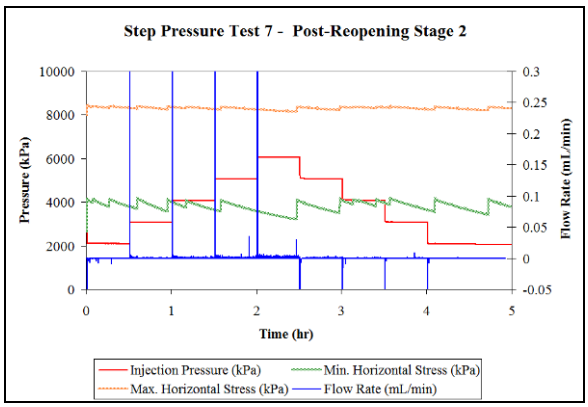

Figure 15: Step pressure test data taken after the second fracture reopening stage.

A comparison of the stepped constant pressure test data obtained before and after the second reopening event is shown in Figure 16. On this plot, it was evident that there was negligible flow rate dependence with pressure after the first fracture reopening stage. This suggested that the flow of the injected fluid was not dominated by stimulated fracture flow and the hydraulic connection between the injection and production boreholes was not flowing effectively if at all. To improve the inter-well connectivity, the second fracture reopening stage was performed with high success. As can be seen in Figure 16, pressure dependent flow rate characteristics were much more prominent after this second stage with a clear proportional relationship. To augment these observations, borehole swabbing was performed periodically to check for fluid production in the intercept borehole. The swabs results did not positively indicate hydraulic connection until after the second fracture reopening stage. Thus, even though the first treatment did not attain an acceptable hydraulic connection, the execution of additional fracture stimulation treatments from the same injection well was successful in creating an effective hydraulic connection.

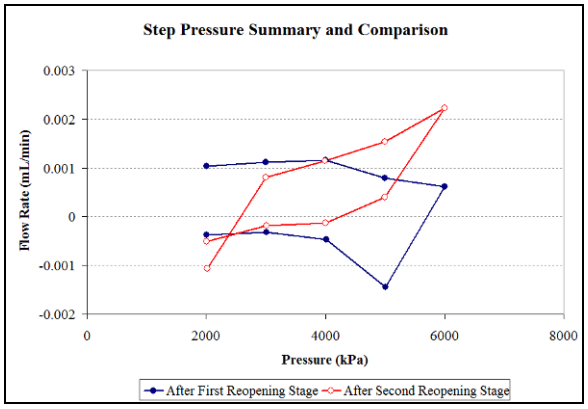

Figure 16: Averaged pressure step data before and after the second fracture reopening stage.

With a confirmed hydraulic connection between the boreholes, the injection fluid was changed to water for thermal flow testing and EGS reservoir characterization. Water injection was performed with constant flow rate control to attain pressure dependent flow characteristics for the reservoir. While this test provides similar data to constant pressure injection, it is more easily compared to field applications where flow rate control is the standard. Periodic borehole swabbing results indicated a significant and continuous fluid production in the intercept borehole. Figure 17 provides an example of the flow rate data obtained during the second water flow test. Here, it is evident that the reduction in viscosity by using water results in significantly reduced pressure losses. Also, these flow rates did not produce any significant AE activity indicating that the stimulated fracture geometry was stable with water flow. Additional testing is required and planned in order to obtain a full characterization of the laboratory simulated EGS reservoir.

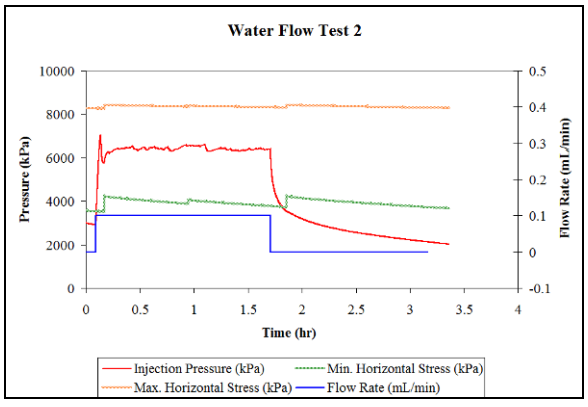

Figure 17: Second water flow test data plot.

4. CONCLUSIONS

A heated true-triaxial cell has successfully been able to produce a laboratory simulation of an EGS reservoir. Preliminary experiments using granite have provided valuable resulting data as well as new observations that may bring some additional insight into the potential of EGS technology. Some of the most important advancements and observations that have been made include:

- The completed development of a heated true-triaxial cell with the ability to simulate multi-well EGS reservoir systems as well as borehole damage by percussively drilling orientated boreholes into a hot stressed sample.
- The successful laboratory simulation of binary injector-producer EGS reservoir in granite with proven fluid communication through a stimulated fracture between two boreholes.
- Multiple hydraulic fracture stimulation treatments may be performed from the same injection borehole to attain significantly increased reservoir conductivity and well fluid communication.
- Significant fracture growth, as indicated by AE activity, is preceded by periods where the real-time second order differential of pressure with time is negative.
- AE source location is a functional and important tool for successful drilling of a production well into a stimulated EGS reservoir.

ACKNOWLEDGEMENTS

Financial support provided by the U.S. Department of Energy under DOE Grant No. DE-FE0002760 is gratefully acknowledged. Also, the Teledyne Isco Renewable Energy Research Grant #1936 was greatly appreciated and enabled the purchase of equipment vital to the success of this project. The opinions expressed in this paper are those of the authors and not the DOE.

REFERENCES

ASTM D341: Standard Practice for Viscosity-Temperature Charts for Liquid Petroleum Products. American Society for Testing and Materials. (2009).

Behrmann, L.A. and Elbel, J.L.: Effect of Perforations on Fracture Initiation. *Journal of Petroleum Technology.* May, (1991).

Clark, J.B.: A hydraulic process for increasing the productivity of wells. *Journal of Petroleum Technology*, Volume 1, Number 1. (1949).

de Pater, C.J., Cleary M.P., Quinn, T.S., Barr, D.T., Johnson, D.E., and Weijers, L.: Experimental Verification of Dimensional Analysis for Hydraulic Fracturing. *SPE Production & Facilities*. November, (1994).

EMI: Orica-4_BTS: Brazilian Tensile Strength Test Datasheet for Orica Core ID 4, Colorado School of Mines Earth Mechanics Institute (EMI). 6 October (2010).

EMI: Orica-4_USG: Uniaxial Compressive Strength Test Datasheet for Orica Core ID 4, Colorado School of Mines Earth Mechanics Institute (EMI). 6 October (2010).

Green, C.A., Barree, R.D., and Miskimins, J. L.: Hydraulic-Fracture-Model Sensitivity Analysis of a Massively Stacked, Lenticular, Tight Gas Reservoir. *SPE Production & Operations*, February. (2009).

Gutierrez, M., Frash, L., and Hampton, J.: Hydraulic Fracturing in Acrylic with Proppant. Available through YouTube at http://youtu.be/rbE4nisWlyA. (2012).

Gutierrez, M., Frash, L., and Hampton, J.: Water Clear Acrylic Laboratory Hydraulic Fracturing Test. Available through YouTube at http://youtu.be/PEXOE2FTDlI. (2012).

Ishida, T., Chen, Q., Mizuta, Y., and Roegiers, J.: Influence of Fluid Viscosity on the Hydraulic Fracturing Mechanism. *Transactions of the ASME*, Volume 126, September. (2004).

Macartney, H., and Morgan, P.: The Potential for Geothermal Energy Recovery from Enhanced Geothermal Systems in the Raton Basin of Southern Colorado, USA. *AAPG Hedberg Geothermal Conference*, Napa, CA, USA. (2011).

Ohtsu, M.: Acoustic Emission Theory for Moment Tensor Analysis. *Research in Nondestructive Evaluation*, Vol. 6, No. 3, pp. 169-184. (1995).

Swenson, D., Schroeder, R., Shinohara, N., and Okabe, T.: Analysis of the Hijiori Long Term Circulation Test. *Proceedings from the Twenty-Fourth Workshop on Geothermal Reservoir Engineering, Stanford University*. Stanford, California. 25-27 January, (1999).

Weijers, L., de Pater, C.J., Owens, K.A., and Kogsbøll, H.H.: Geometry of Hydraulic Fractures Induced From Horizontal Wellbores. *SPE Production and Facilities*, May. (1994).

Wieland, C.W., Miskimins, J.L., Black A.D., and Green S.J.: Results of a Laboratory Propellant Fracturing Test in a Colton Sandstone Block. SPE Annual Technical Conference and Exhibition, San Antonio, Texas, USA, 24-27 September. (2006).